

**Project Report  
NTI-4**

# **Unified Synthetic Aperture Space Time Adaptive Radar (USASTAR) Concept**

**J.K. Jao  
A.F. Yegulalp  
S. Ayasli**

**24 May 2004**

---

**Lincoln Laboratory**  
MASSACHUSETTS INSTITUTE OF TECHNOLOGY  
*LExINGTON, MASSACHUSETTS*



---

Prepared for the Department of the Air Force under Contract F19628-00-C-0002.

Approved for public release; distribution is unlimited.

**BEST AVAILABLE COPY**

**20040601 037**

18 November 2004

## ERRATA

Document: Project Report NTI-4, "Unified Synthetic Aperture Space Time Adaptive Radar (USASTAR) Concept," dated 24 May 2004

Please make the following changes to your copy of the above report:

**INTRODUCTION – Page 1, paragraph 4, lines 2–4**

Change:

The USASTAR technique can be applied to radar operating at any frequency band from Ku to VHF, though in this report only X-band and UHF band applications are presented.

To:

The USASTAR technique can be applied to radar operating at any frequency band from Ku to VHF. In this report, the results of a few UHF and L-band numerical examples and one X-band field experiment are presented.

**Figure 12 caption – Page 15**

Change:

Figure 12. Estimated SINR loss for example USASTAR parameters at X-band.

To:

Figure 12. Estimated SINR loss for one L-band example.

A 423144

*Publications Office*  
MIT Lincoln Laboratory  
244 Wood Street  
Lexington, MA 02420

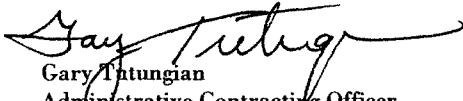
This report is based on studies performed at Lincoln Laboratory, a center for research operated by Massachusetts Institute of Technology. This work was sponsored by the Department of the Air Force, ESC/XPK, under Contract F19628-00-C-0002.

This report may be reproduced to satisfy needs of U.S. Government agencies.

The ESC Public Affairs Office has reviewed this report, and it is releasable to the National Technical Information Service, where it will be available to the general public, including foreign nationals.

This technical report has been reviewed and is approved for publication.

FOR THE COMMANDER

  
Gary Tintungian  
Administrative Contracting Officer  
Plans and Programs Directorate  
Contracted Support Management

Non-Lincoln Recipients

PLEASE DO NOT RETURN

Permission is given to destroy this document  
when it is no longer needed.

**Massachusetts Institute of Technology  
Lincoln Laboratory**

**Unified Synthetic Aperture Space Time Adaptive Radar (USASTAR)  
Concept**

*J.K. Jao  
A.F. Yegulalp  
S. Ayasli  
Group 104*

**Project Report NTI-4**

**24 May 2004**

**Approved for public release; distribution is unlimited.**

**Lexington**

**Massachusetts**

## ABSTRACT

A novel airborne GMTI radar approach based on adaptive multichannel SAR processing is proposed to improve the surface surveillance sensor performance in detecting slowly moving targets on the ground. The key sensor attributes are broad bandwidth, large antenna array baseline of multiple phase centers, and adaptive array processing over a long coherent integration time interval. This sensor architecture may improve the GMTI sensor capabilities in several aspects

- 1) Target detection at very low minimum detectable velocity (MDV)
- 2) Robust adaptive processing to cancel strong ground clutter
- 3) High sensitivity to detect weak targets
- 4) Flexible array requirement including sparser arrays
- 5) Compatibility with SAR imaging applications.

The presented sensor architecture is suitable for deployment on a fast, stand-off airborne surveillance platform against weak and slow targets such as dismounted troops, guerrillas, terrorists, and illegal vehicle or boat traffic, both in the clear and under concealment.

## TABLE OF CONTENTS

	<b>Page</b>
Abstract	iii
List of Illustrations	v
1. INTRODUCTION	1
2. THE USASTAR CONCEPT	3
3. USASTAR FORMULATION AND PERFORMANCE PREDICTIONS	5
3.1 SNR Loss in Long-CPI Processing	5
3.2 Computational Examples	8
3.3 SAR-Based Analysis and Computational Examples	12
4. HIGH-RESOLUTION ADAPTIVE ARRAY PROCESSING APPROACHES	17
4.1 Single-Cell Adaptive Matched Filtering with “Local” Array Calibration	18
4.2 Array Response Calibration	20
4.3 Single-Cell Adaptive Matched Filtering with “Global” Array Calibration	20
4.4 Multiple-Cell Space-Fast-Time Adaptive Matched Filtering	21
4.5 Multiple-Pixel Adaptive SAR Image Processing	22
4.6 Sample Radar Measurement Results	23
5. SUMMARY	25
REFERENCES	27

## LIST OF ILLUSTRATIONS

Figure No.		Page
1	USASTAR concept.	3
2	SNR array loss compared with two separate subarray apertures.	10
3	SNR array loss of two sample cases.	11
4	SNR array loss for two clutter levels.	11
5	USASTAR SAR preprocessing concept.	12
6	Properties of SAR preprocessing.	12
7	Theoretical formula for SAR steering vector.	13
8	Theoretical formula for USASTAR steering vector.	13
9	Simplifying assumptions for theoretical SNR loss performance predictions.	14
10	Theoretical formulas for USASTAR SINR loss.	14
11	SINR loss estimate for conventional GMTI.	14
12	Estimated SINR loss for example USASTAR parameters at X-band.	15
13	Estimated SINR loss for three different sets of radar parameters at UHF.	15
14	USASTAR SINR loss predictions showing the effect of extending the antenna baseline with a towed aperture 300 m behind the first antenna element, at UHF.	16
15	Sample output of the multiple-cell adaptive processing derived from the Tuxedo data set No. 1916 over a test area.	24

# 1. INTRODUCTION

This report describes a novel radar and processing concept that addresses wide-area, standoff surveillance and detection against dismounted troops, guerrillas, terrorists, or illegal vehicle or boat traffic, both in the clear and under concealment. What makes this problem difficult comes from a combination of factors.

1. Targets of interest listed above are generally small, may have very small Doppler signatures, and may be concealed in trees or in terrain clutter.
2. Large standoff ranges are desirable to keep the surveillance as covert and as safe as possible.
3. Areas to be searched can be very large and large area surveillance rates are needed.
4. To catch the enemy or the targets in action or in exploitable conditions, persistent coverage is needed which requires all weather, day, and night sensing capability.

Current microwave surveillance systems can provide all weather, day and night, rapid and wide area coverage surveillance capabilities against vehicle size, and stationary or moving targets in clear but will be limited in performance against the small, slow and concealed targets listed above. Synthetic aperture radar (SAR) is commonly used for stationary target detection and space-time adaptive processing (STAP) ground moving target indicator (GMTI) methods have been developed for moving target detection. Standard SAR use a single phase-center antenna, wideband waveforms, and long coherent integration times to achieve high resolution. Moving targets typically appear smeared in SAR images. While algorithms have been developed [1–3] to refocus target returns in SAR images, a single phase center SAR is inherently limited in clutter cancellation due to lack of spatial degrees of freedom (DoF). STAP GMTI, on the other hand, uses multiple phase centers, which provide the spatial DoF needed for clutter cancellation, but uses narrowband waveforms, and short coherent integration times, which limit performance against very small and slow targets.

This report describes a unified multichannel wideband, long CPI (coherent integration interval) radar concept, USASTAR (unified synthetic aperture space time adaptive radar), for fixed wing aircraft such as Global Hawk, Predator, or manned aircraft, that combines the advantages of both the high resolution SAR and multichannel STAP techniques to fill in the technology gap mentioned.

By unifying the SAR and GMTI properties, this radar concept offers a potential capability to detect stationary and moving ground targets at arbitrary speed and geometry. The USASTAR technique can be applied to radar operating at any frequency band from Ku to VHF, though in this report only X-band and UHF band applications are presented. While the X-band application can provide the desired higher resolution for target discrimination when targets are in the clear, the UHF application provides penetration through some concealment such as foliage, camouflage, and certain kind of walls.



## 2. THE USASTAR CONCEPT

Detection of moving targets by airborne radar is generally accomplished by multiple phase centers and STAP to cancel clutter which spreads in Doppler due to the aircraft motion. As target velocity becomes smaller, achieving acceptable performance requires very large antennas, very slow or stationary platforms, or much higher resolution to reduce clutter. An approach used today and in the past is to install a pulse-Doppler radar on a stationary (or nearly stationary) platform. The new concept proposed here is based on a faster flying aircraft, providing larger standoff range and larger surveillance rates, with a very long antenna baseline, and higher resolution.

USASTAR is based on adaptive clutter cancellation and coherent change detection using multiple phase centers on the same platform (or multiple platforms connected with a high precision geotracking system such as laser geodimeter), each producing a SAR image or a high-resolution range-Doppler map data, where the time it takes for the platform to travel the distance between the phase centers is sufficient for targets to move a number of cells (USASTAR can be used even when targets move a fraction of a cell using target phase change, but with more target loss). USASTAR is an approach to GMTI when target Doppler is expected to be very low. It also provides simultaneous capability for SAR imaging and detection of stationary targets and GMTI detection of moving targets. The concept is illustrated in Figure 1.

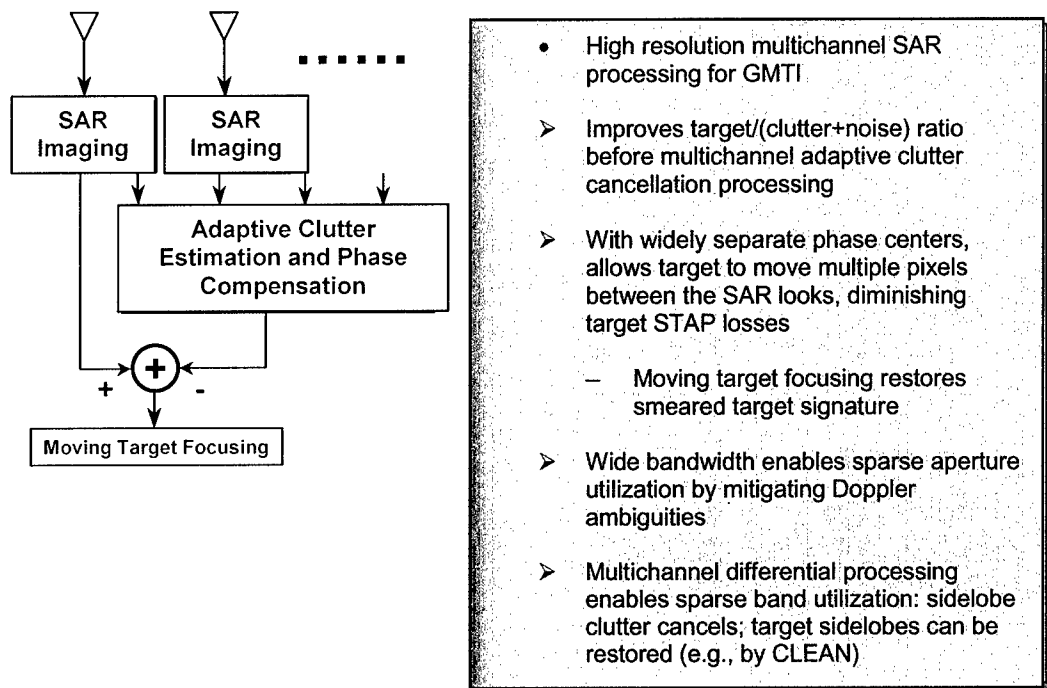


Figure 1. USASTAR concept.

It is expected that USASTAR will provide improved clutter cancellation and sensitivity, as compared to existing SAR change detection or GMTI systems, in detecting small and slow movers such as dismounts. USASTAR can achieve this improvement over conventional SAR pass-to-pass change detection by providing better registered images from multiple phase centers on the same platform and by reducing the time between the radar looks (depending on the length of the baseline and the speed of the aircraft), thereby reducing the uncorrelated clutter returns between the various looks. Because USASTAR

produces multiple channel high-resolution SAR or range-Doppler map data, more clutter sample data are available for local adaptation and training of adaptive array processing algorithms used in GMTI processing. Thus, the USASTAR approach enables more accurate in-situ data-driven array calibration, better mitigation of array-airframe interactions, and higher cancellation of strong, inhomogeneous clutter in realistic field environments, compared to conventional GMTI systems.

In the following sections two alternative formulations of the USASTAR concept and predicted results are presented. Also presented is a sample result from application of the method to Lockheed Martin Tuxedo X-band SAR data [4].

### 3. USASTAR FORMULATION AND PERFORMANCE PREDICTIONS

Theoretical tools have been developed to help define optimal USASTAR system architecture and parameters. The key USASTAR system attributes are broad bandwidth large antenna array baseline, and long coherent integration time (CPI). Both bandwidth and array structure are important system design parameters that need to be carefully selected to trade off the intended system performance goal in operational utility and functionality against the system complexity and cost. These two parameters significantly affect radar system performance in suppressing radio interference, jamming, and clutter. Furthermore, long CPI enhances radar Doppler (or cross-range) resolution that is essential to increase radar target detection sensitivity and clutter suppression performance. For GMTI radar, the ability to cancel strong clutter is a prerequisite to reliable detection of slowly moving targets. In radar design, the trade-off analysis of adaptive array, signal processing, and performance typically relies on numerical simulation. While computer simulations may be useful in some circumstance, this approach may demand substantial computational resource to simulate a system characterized by a large bandwidth and a large array of many DoFs. In the latter situation, it will be very desirable to have analytic tools that can accurately and efficiently predict the system performance in clutter cancellation. For this purpose, this section will present a set of analytic formula that may be used to compute the radar clutter cancellation performance in terms of a given radar waveform in its signal frequency composition and bandwidth and of an array structure in its element placement and aperture.

#### 3.1 SNR LOSS IN LONG-CPI PROCESSING

A set of closed-form expressions have been derived that specify the theoretical lower bound of the signal-to-noise ratio (SNR) loss incurred in the clutter cancellation via adaptive array processing. The radar parameters and assumptions used in the theoretical development are defined as follows.

Here, the velocity of the airborne radar aircraft is assumed to be  $v_a$  moving along a straight line parallel to a linear radar-receiving array. The linear array consists of  $N$  array sensor elements whose phase centers are located at  $D_n$ ,  $n = 0, 1, 2, \dots, N - 1$  as measured from a reference location such as the phase center of a separate radar transmitter antenna. The placement of the  $N$  sensor elements can be arbitrarily distributed within the linear array aperture  $D$  that may be sparse or only partially populated. In order to minimize the SNR loss in adaptive clutter cancellation, radar target signal integration will be carried out over a long CPI. In this limit, the CPI will be longer than the time of radar flight over the entire array aperture length  $D$ ,  $CPI \gg D/v_a$ . As target migration is expected over a long CPI due to range-walk of a moving target and its signal smearing cross multiple Doppler filters, proper target motion compensation will be assumed to avoid any target signal loss incurred in integration. The radar waveform is characterized by a spectrum  $p_B(\nu)$  that spans a frequency band  $[-B/2, B/2]$  center at  $f_0$ . The signal spectrum  $p_B(\nu)$  may be arbitrary and sparse in its spectral occupation within the fractional bandwidth  $B_f = B/f_0$ . However, the spectrum is known such that perfect range compression or matched filtering of the pulse signal is feasible.

Given these parameters, the SNR loss at the target radial velocity  $\nu$  incurred by an optimal array processor in nulling clutter, that is characterized by the wind-blown internal clutter motion (ICM) spectrum  $p_{ICM}(\nu)$ , can be shown to be

$$\begin{aligned}
\text{SNR loss} &= \bar{\mathbf{t}}^H \mathbf{R}_{CN}^{-1}(\nu) \bar{\mathbf{t}} \quad ; \\
\mathbf{R}_{CN}(\nu) &= (\text{CNR}) \phi^2 \int_{-\infty}^{\infty} p_{ICM}(u - \nu) \bar{\mathbf{c}}(u) \bar{\mathbf{c}}^H(u) du + \mathbf{I}_N \quad ; \\
\text{Target vector } [\bar{\mathbf{t}}]_n &= \frac{1}{\sqrt{N}} \quad , \quad \text{clutter vector } [\bar{\mathbf{c}}(\nu)]_n = \frac{\phi_n(\nu)}{\phi} \quad .
\end{aligned} \tag{3.1}$$

Here, the  $\mathbf{t}$  is the target steering vector and  $\mathbf{R}_{CN}(\nu)$  is the clutter-plus-noise covariance matrix that can be expressed as the convolution of the wind-blown clutter ICM spectrum  $p_{ICM}(\nu)$  and the outer product of  $\mathbf{c}(\nu)$ . The latter quantity is actually the clutter-plus-noise covariance in the absence of any clutter spread due to internal clutter motion and is a function of  $\phi(\nu)$ .

$$\begin{aligned}
\phi_n(\nu) &= \exp(-j\omega_d \tau_n) \int_{\text{Band}} p_B(\nu) \exp\left(-j\omega_d \tau_n B_f \frac{\nu}{B}\right) d\nu \quad , \quad \phi^2 = \sum_{n=0}^{N-1} |\phi_n(\nu)|^2 \quad . \\
\omega_0 &= 2\pi f_0 \quad , \quad k_0 = \frac{2\pi}{\lambda_0} \quad , \quad \omega_d = 2k_0 v \quad ; \quad \tau_n = \frac{D_n}{2v_a} \quad , \quad B_f = \frac{B}{f_0} \quad .
\end{aligned} \tag{3.2}$$

The function  $\phi(\nu)$  is related to the Fourier transform of the waveform spectrum  $p_B(\nu)$  and its functional forms for two special cases, the constant and the Gaussian spectra, are given as follows

$$\begin{aligned}
\phi_n &= \exp(-j\omega_d \tau_n) \frac{\sin(\omega_d \tau_n B_f / 2)}{\omega_d \tau_n B_f / 2} \\
&\text{for constant spectrum } p_B(\nu) = \frac{1}{B} \quad . \\
\phi_n &= \exp(-j\omega_d \tau_n) \exp\left[-\left(\frac{\omega_d \tau_n B_f}{4\pi}\right)^2\right] \\
&\text{for Gaussian spectrum } p_B(\nu) = \frac{2}{\sqrt{\pi}B} \exp\left(-\frac{4\nu^2}{B^2}\right) \quad .
\end{aligned} \tag{3.3}$$

The clutter ICM spectrum  $p_{ICM}(\nu)$  is composed of two components, the DC part  $\delta(\nu)$  and the AC spectrum  $p_{AC}(\nu)$  due to motion modulation:

$$\begin{aligned}
\text{Clutter ICM spectrum } p_{ICM}(\nu) &= \frac{r}{r+1} \delta(\nu) + \frac{1}{r+1} p_{AC}(\nu) \quad ; \\
\text{Clutter correlatoin } \rho_{ICM}(\tau) &= \int_{-\infty}^{\infty} p_{ICM}(\nu) \exp(j2k_0 v \tau) d\nu \quad .
\end{aligned} \tag{3.4}$$

One popular model is to employ an exponential spectrum or its corresponding temporal correlation function  $\rho_{ICM}(\tau)$  to characterize the clutter ICM

$$\begin{aligned}
&\text{Exponential ICM spectrum: } p_{AC}(v) = \frac{1}{2\beta_v} \exp\left(-\frac{|v|}{\beta_v}\right), \\
&\text{Clutter correlatoin: } \rho_{ICM}(\tau) = \frac{r}{r+1} + \frac{1}{r+1} \frac{1}{1+4k_0^2\beta_v^2\tau^2}; \\
&\text{DC/AC power ratio } r: \\
&\quad 10\log_{10} r = 63.2 - 12.1\log_{10}(\text{Frequency, MHz}) \\
&\quad \quad - 15.5\log_{10}(\text{Wind speed, mph}) \\
&\text{Clutter spread: } \beta_v = 0.1048(\log_{10}(\text{wind speed, mph}) + 0.4147) \text{ m/s}.
\end{aligned} \tag{3.5}$$

In Equation (3.5), both functional parameters, the DC/AC power ratio  $r$ , and the root mean square (rms) spectral spread  $\beta_v$ , are dependent on the surface wind speed. Unfortunately, the exponential clutter ICM model does not render Equation (3.1) into a mathematically tractable form. Thus, for the reason of obtaining a mathematical formula convenient for computation, an equivalent Gaussian ICM model is sometime preferred. This model is defined by

$$\begin{aligned}
&\text{Gaussian ICM spectrum: } p_{AC}(v) = \frac{1}{\sqrt{2\pi}\beta_v} \exp\left(-\frac{v^2}{2\beta_v^2}\right), \\
&\text{Clutter correlation: } \rho_{AC}(\tau) = \exp(-2k_0^2\beta_v^2\tau^2).
\end{aligned} \tag{3.6}$$

The clutter spread parameter  $\beta_v$  for the Gaussian ICM spectrum typically must assume a much larger value than the corresponding  $\beta_v$  used in the exponential model in order to result in comparable SNR loss results as predicted by Equation (3.1). By assuming both a Gaussian clutter ICM and a Gaussian waveform spectra, a closed form expression for the clutter-plus-noise covariance function  $R_{CN}(v)$  of Equation (3.1) can be obtained for this special case as

$$\begin{aligned}
[R_{ICM}]_{mn} &= (CNR)\phi^2 \left\{ \frac{r}{r+1} [\bar{c}(v)\bar{c}^H(v)]_{mn} \right. \\
&\quad \left. + \frac{\sqrt{G_{mn}}}{r+1} ([\bar{c}(v)\bar{c}^H(v)]_{mn} \rho_{AC}(\tau_n - \tau_m))^{G_{mn}} \right\} + \delta_{mn}; \\
G_{mn} &= [1 + 0.5(B_f k_0 \beta_v)^2 (\tau_m^2 + \tau_n^2)]^{-1}.
\end{aligned} \tag{3.7}$$

Also, the following approximation of  $R_{CN}(v)$  is useful for narrowband waveforms

$$\begin{aligned}
R_{CN}(v) &= (CNR)\phi^2 \int_{-\infty}^{\infty} p_{ICM}(u-v) \bar{c}(u) \bar{c}^H(u) du + I_N \\
&\cong (CNR)\phi^2 \bar{c}(v) \bar{c}^H(v) \odot R_{ICM} + I_N, \\
&\quad \text{for } k_0 \beta_v B_f \max(\tau_n) \ll 1; \\
[R_{ICM}]_{mn} &= \rho_{ICM}(\tau_n - \tau_m).
\end{aligned} \tag{3.8}$$

In the absence of any wind-blown clutter modulation, Equation (3.1) may be considerably simplified as

$$\text{SNR loss} = 1 - \frac{(CNR)\phi^2}{1 + (CNR)\phi^2} |\bar{\mathbf{t}}^H \bar{\mathbf{c}}|^2 \quad ; \quad \bar{\mathbf{t}}^H \bar{\mathbf{c}} = \frac{1}{\sqrt{N}\phi} \sum_{n=0}^{N-1} \phi_n(v) \quad . \quad (3.9)$$

In this situation, the SNR loss may be obtained from Equations (3.2) and (3.3) by substituting the following inner product of  $\mathbf{t}$  and  $\mathbf{c}$  into Equation (3.9):

$$\begin{aligned} \bar{\mathbf{t}}^H \bar{\mathbf{c}} &= \frac{1}{N} \sum_{n=0}^{N-1} \exp(-j2\pi f_0 t_n) \frac{\sin(\pi B t_n)}{\pi B t_n} \\ \text{for constant spectrum } p_B(v) &= \frac{1}{B} \quad , \quad t_n = \frac{D_n v}{C v_a} \quad , \quad C \text{ is the light velocity.} \\ \bar{\mathbf{t}}^H \bar{\mathbf{c}} &= \frac{1}{N} \sum_{n=0}^{N-1} \exp(-j2\pi f_0 t_n) \exp\left(-\frac{B^2 t_n^2}{4}\right) \\ \text{for Gaussian spectrum } p_B(v) &= \frac{2}{\sqrt{\pi} B} \exp\left(-\frac{4v^2}{B^2}\right) . \end{aligned} \quad (3.10)$$

These equations also may be modified to accommodate a waveform spectrum that may span several non-overlapping subbands within the system bandwidth  $B$ . For example, if there are  $M$  separate subbands  $b_m$  individually centered at  $f_m$ ,  $m = 0, 1, \dots, M-1$  within  $B$ , each with a constant power spectral density  $1/B_M$ ,  $B_M = b_0 + b_1 \dots + b_{M-1}$ , then Equation (3.10) becomes

$$\begin{aligned} \bar{\mathbf{t}}^H \bar{\mathbf{c}} &= \sum_{m=0}^{M-1} \frac{1}{N} \sum_{n=0}^{N-1} \exp(-j2\pi f_m t_n) \frac{\sin(\pi b_m t_n)}{\pi b_m t_n} \quad ; \\ p_B(v) &= \sum_{m=0}^{M-1} p_m(v) \quad , \quad p_m(v) = \frac{1}{B_M} \quad , \quad m = 0, 1, \dots, M-1 \quad \text{and} \\ v &\in [f_m - 0.5b_m, f_m + 0.5b_m] \in [f_0 - 0.5B, f_0 + 0.5B] \quad , \quad B_M = \sum_{m=0}^{M-1} b_m \quad . \end{aligned} \quad (3.11)$$

### 3.2 COMPUTATIONAL EXAMPLES

Theoretical SNR loss due to the clutter residue as the output of an imperfect clutter nulling process are plotted in Figures 2 through 4 for a few sample cases. These figures illustrate the SNR loss dependence on array structure, bandwidth, radar speed, clutter strength, and wind speed. Generally speaking, a low SNR loss indicates good clutter cancellation and better adaptive array processing performance that results in a lower minimal discernible detectable velocity of a moving target. By inspecting these figures, it is clear that the best results are achieved by using an array with a long aperture baseline and a large bandwidth to suppress the periodic loss due to the grating lobe effects when the array is only populated by sparse elements distributed over a large aperture.

Figure 2 compares the SNR loss of an array with two separate subarray apertures operated with either the narrowband mode shown in red in Figure 2(a), or the broadband mode, shown in green in Figure 2(b), with a bandwidth of 200 MHz centered at 300 MHz. Two array structures are illustrated.

The first is a filled array of 101 elements spanning a total array length of 50 m. The second is a sparse array consisting of two subarrays separated by 40 m. Each subarray has 11 antenna elements in half-wavelength spacing over a span of 5 m. For reference, the SNR loss curves for a filled array are also plotted; one is for the case of a stationary radar (in black) whereas the other an airborne radar moving at the speed of 50 m/s (in blue). In these charts, the solid curves are modeled by assuming an Gaussian clutter ICM spectrum for a very windy condition at the speed of 20 mph such that the DC-to-AC ratio  $r$  is 11.1 dB and the rms clutter spread  $\beta_v$  is 0.4 m/s. The ideal cases in the absence of wind are plotted in dashed curves.

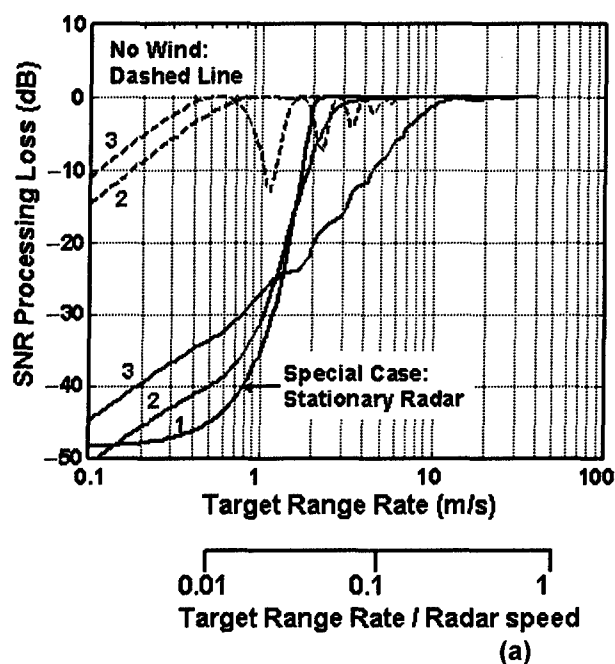
Figure 3 compares the SNR loss of two sample cases. The first case (in red) is generated for a short array aperture of 4 m in length and is operated over a 20 MHz bandwidth between 380 and 400 MHz. While the second case (in green) assumes two subarray apertures, each of 2 m in length, separated by 500 m but the radar band spans from 200 to 400 MHz. The radar speeds for both cases are taken to be 50 m/s. Due to the different bandwidth and consequently different range resolution, the element clutter to noise ratio (CNR) of 50 dB for the first case is 10 dB stronger than that of the second case. Also, the wind-blown clutter ICM spectrum is taken as Gaussian. At the surface wind speeds of 5 mph and 20 mph, respectively, the ICM DC-to-AC ratios are 20 dB and 11.1 dB, respectively, and the rms clutter spread  $\beta_v$  are 0.2 m/s and 0.4 m/s.

Figure 4 compares the difference in SNR loss for two clutter levels. In this exercise, the radar moves at a much faster speed of 200 m/s. The array consists of two small subarrays of two wavelengths, or five elements separated by 500 m. The radar frequency band spans from 200 to 400 MHz. The same wind-blown clutter ICM model is used as that for Figure 3. As clearly shown by this figure, the SNR loss in the presence of a lower clutter level at the element CNR of 20 dB are clearly smaller than the corresponding cases at the element CNR of 40 dB.

### 3.3 SAR-BASED ANALYSIS AND COMPUTATIONAL EXAMPLES

In this section, an alternative formulation of the USASTAR processing concept and predicted performance, as measured by signal-to-interference noise ratio (SINR) loss factor, will be presented. In this formulation, the long CPI wideband Doppler processing will be treated as SAR processing, and the USASTAR concept will be treated as adaptive processing of multichannel SAR images [5]. Effects due to clutter internal motion are not included here, but could be added along the same lines as in the previous analysis.

Figures 5 through 14 show the properties associated with SAR processing prior to spatial adaptive processing, theoretical formulas for SAR and USASTAR steering vectors and predicted SINR loss performance, under simplifying assumptions shown, compared to conventional GMTI. Both X-band and UHF examples are given.



Radar speed: 50 m/s  
Element CNR: 40 dB

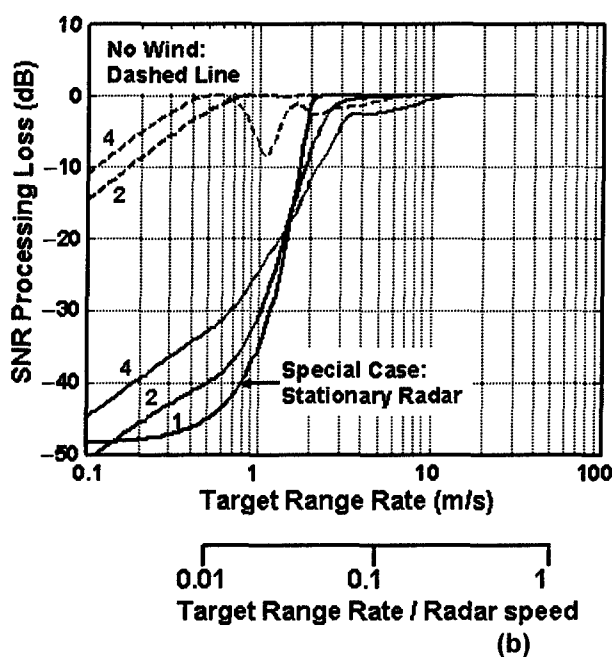
Center frequency: 300 MHz  
Bandwidth  
Narrowband (black and blue)

Linear array phase centers

- 1) 101 at  $[0 : 0.5 : 50] \lambda$   
(stationary platform)
- 2) 101 at  $[0 : 0.5 : 50] \lambda$
- 3) 22 at  $[0 : 0.5 : 5]$   
and  $[45 : 0.5 : 50] \lambda$

Clutter ICM model

Dashed line: no wind  
Solid line  
20 mph, Gaussian spectrum  
DC/AC: 11.1 dB  
RMS spread: 0.4 m/s



Radar speed: 50 m/s  
Element CNR: 40 dB

Center frequency: 300 MHz  
Bandwidth  
Narrow band (black and blue)  
200 MHz (green)

Linear array phase centers:

- 1) 101 at  $[0 : 0.5 : 50] \lambda$   
(stationary platform)
- 2) 101 at  $[0 : 0.5 : 50] \lambda$
- 4) 22 at  $[0 : 0.5 : 5]$   
and  $[45 : 0.5 : 50] \lambda$

Clutter ICM model

Dashed line: no wind  
Solid line  
20 mph, Gaussian spectrum  
DC/AC: 11.1 dB  
RMS spread: 0.4 m/s

Figure 2. SNR array loss compared with two separate subarray apertures operated with (a) narrowband mode, or (b) broadband mode.



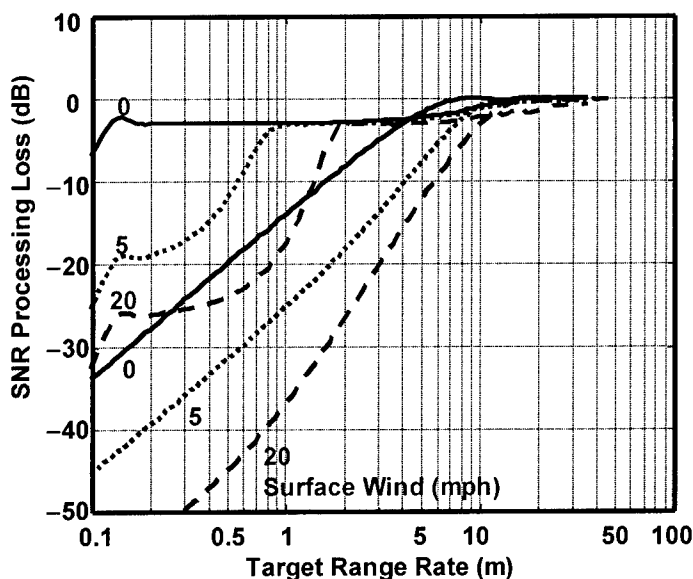


Figure 3. SNR array loss for two sample cases.

Platform speed: 50 m/s  
Long CPI ( $\gg D/V \sim 10$  s)

Clutter ICM model:  
Gaussian spectrum  
Wind speed: 0, 5, 20 mph

#### Array structure

- Single, filled array:
  - One 4 m aperture
  - Band: 380–400 MHz
  - CNR: 50 dB
- Two sparse arrays:
  - Two 2 m apertures, 500 m separation
  - Band: 200–400 MHz
  - CNR: 40 dB

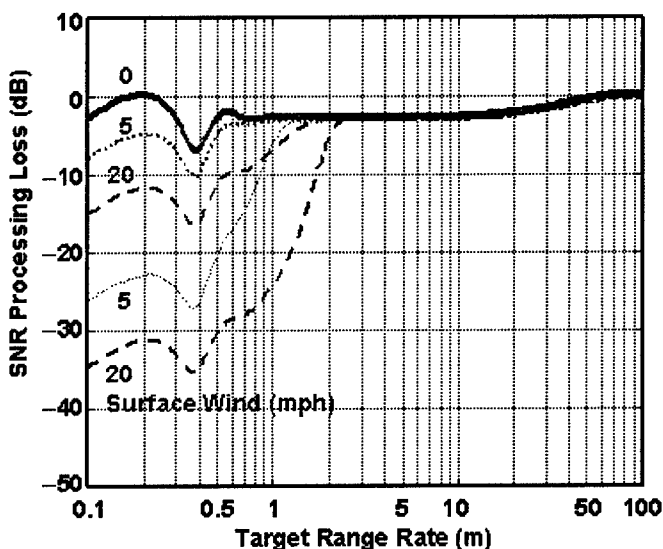


Figure 4. SNR array loss for two clutter levels.

Radar speed: 200 m/s  
Frequency band: 200–400 MHz

Linear array:  
2 small filled apertures,  
each has 5 elements  
Element spacing:  $0.5 \lambda$   
Aperture separation: 500 m

Array element CNR:  
20 and 40 dB

Clutter ICM spectrum:  
Gaussian spectrum  
Wind:

Solid line: No wind  
Dotted line: 5 mph  
Dashed line: 20 mph

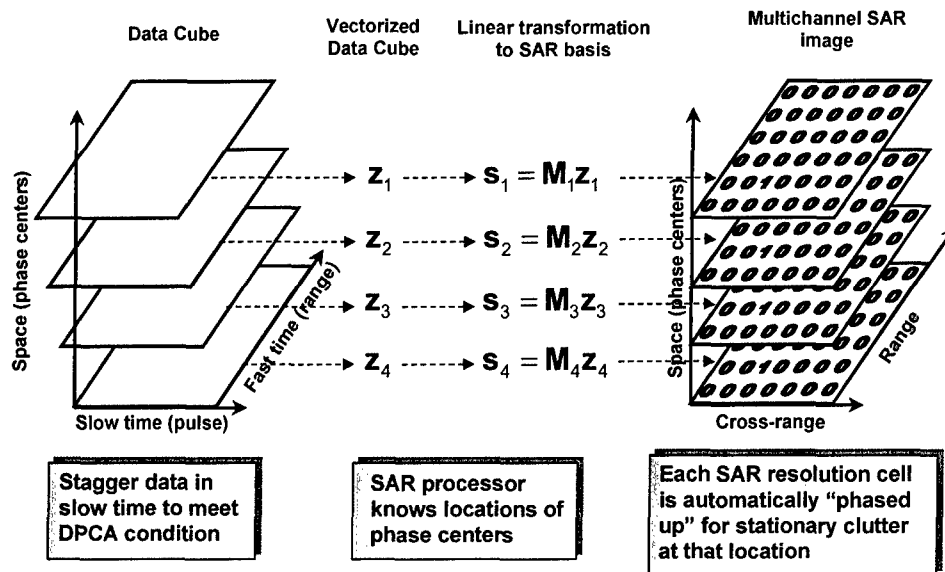


Figure 5. USASTAR SAR preprocessing concept.

- SAR is the wideband, long-CPI generalization of the Doppler processor in ordinary post-Doppler STAP
- Linear transform of input data cube
  - Annihilates the exoclutter subspace
  - Invertible transformation of the endoclutter subspace
- "Freezes" clutter into SAR resolution bins
  - Clutter in one bin is well-decorrelated from other bins multiple resolution cells away.
  - Stationary targets have trivial steering vectors
  - Stationary clutter has trivial covariance
- Moving targets smear over multiple resolution cells

Figure 6. Properties of SAR preprocessing.

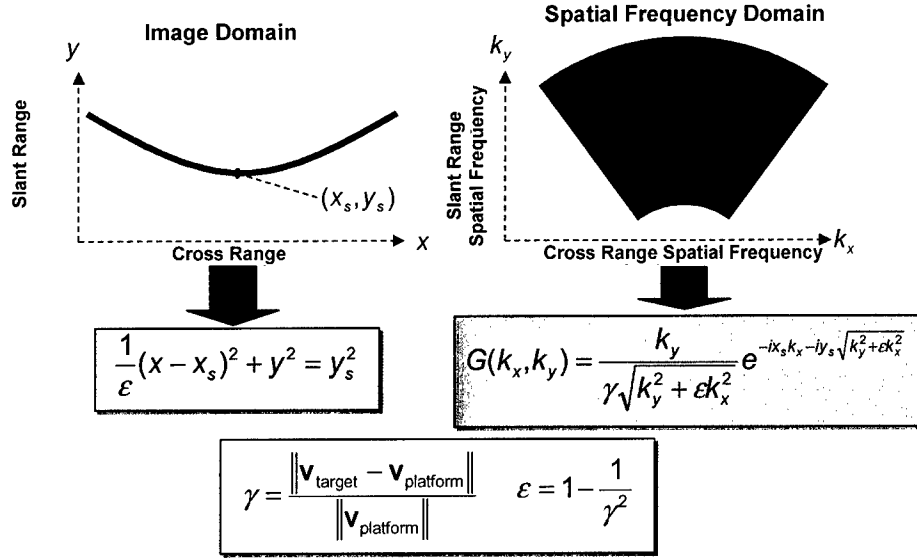


Figure 7. Theoretical formula for SAR steering vector.

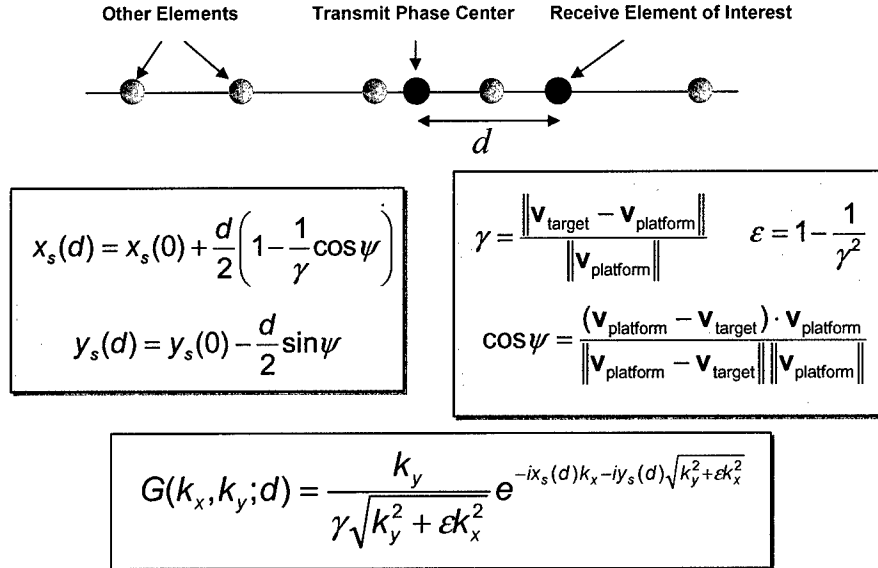


Figure 8. Theoretical formula for USASTAR steering vector.

- Large clutter-to-noise ratio
- Elements are mutually calibrated
- No internal clutter motion, crab, unmeasured aircraft motion and vibration
- No jammers and other interference
- Isotropic element patterns
- Optimal AMF processing with perfect knowledge of steering vectors and clutter covariance

Figure 9. Simplifying assumptions for theoretical SINR loss performance predictions.

Target Steering Vector

$$\mathbf{u} = \sum_{n=1}^N \mathbf{v}(n) \otimes \mathbf{e}(n)$$

Vectorized Target Image From  $N$ -th Channel

Element Space Basis Vector

$$\mathbf{e}(1) = \begin{pmatrix} 1 \\ 0 \\ 0 \\ \vdots \\ 0 \end{pmatrix}, \mathbf{e}(2) = \begin{pmatrix} 0 \\ 1 \\ 0 \\ \vdots \\ 0 \end{pmatrix}, \dots, \mathbf{e}(N) = \begin{pmatrix} 0 \\ 0 \\ 0 \\ \vdots \\ 1 \end{pmatrix}$$

Clutter + Noise Covariance

$$\mathbf{R} = \sigma_n^2 \mathbf{I} + \mathbf{R}_c \otimes \mathbf{e}\mathbf{e}^H$$

Noise Power

Clutter Pixel-space Covariance

$$\mathbf{e} = \sum_{n=1}^N \mathbf{e}(n)$$

Inverse Covariance

$$\mathbf{R}^{-1} = \frac{1}{\sigma_n^2} \mathbf{I} \otimes \mathbf{I} - \frac{1}{\sigma_n^4} \left( \mathbf{R}_c \left( \mathbf{I} + \frac{N}{\sigma_n^2} \mathbf{R}_c \right)^{-1} \right) \otimes \mathbf{e}\mathbf{e}^H$$

Large Clutter-to-noise Limit

$$\sigma_n^2 \mathbf{R}^{-1} \xrightarrow{\sigma_n^2 \rightarrow 0} \mathbf{I} \otimes \mathbf{I} - \frac{1}{N} \mathbf{I} \otimes \mathbf{e}\mathbf{e}^H$$

SINR Loss

$$\sigma_n^2 \frac{\mathbf{u}^H \mathbf{R}^{-1} \mathbf{u}}{\mathbf{u}^H \mathbf{u}} = 1 - \frac{\left\| \sum_{n=1}^N \mathbf{v}(n) \right\|^2}{N \sum_{n=1}^N \left\| \mathbf{v}(n) \right\|^2}$$

Figure 10. Theoretical formulas for USASTAR SINR loss.

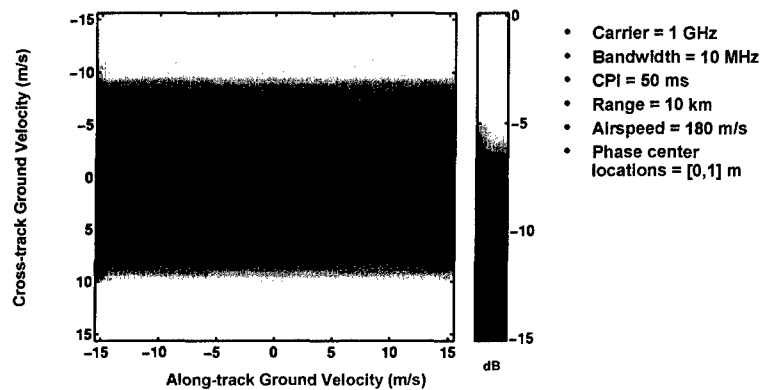


Figure 11. SINR loss estimate for conventional GMTI.

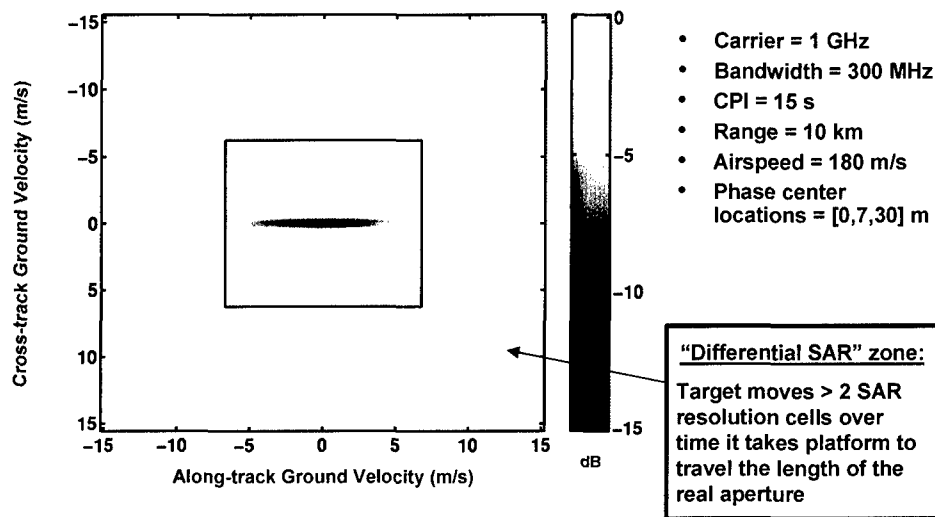


Figure 12. Estimated SINR loss for example USASTAR parameters at X-band.

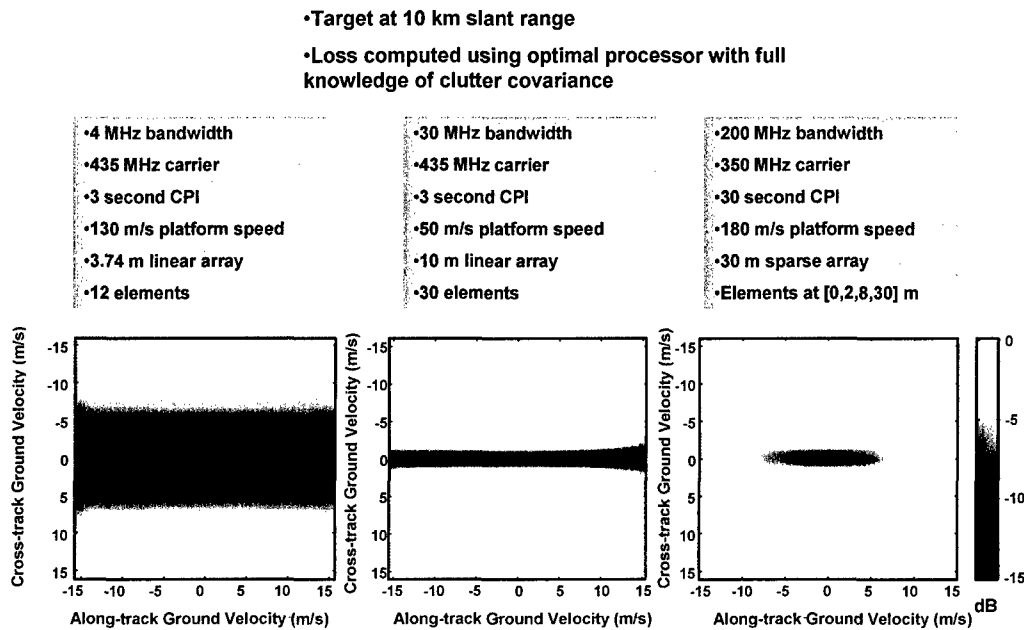


Figure 13. Estimated SINR loss for three different sets of radar parameters at UHF.

- Target at 10 km slant range
- Loss computed using optimal processor with full knowledge of clutter covariance

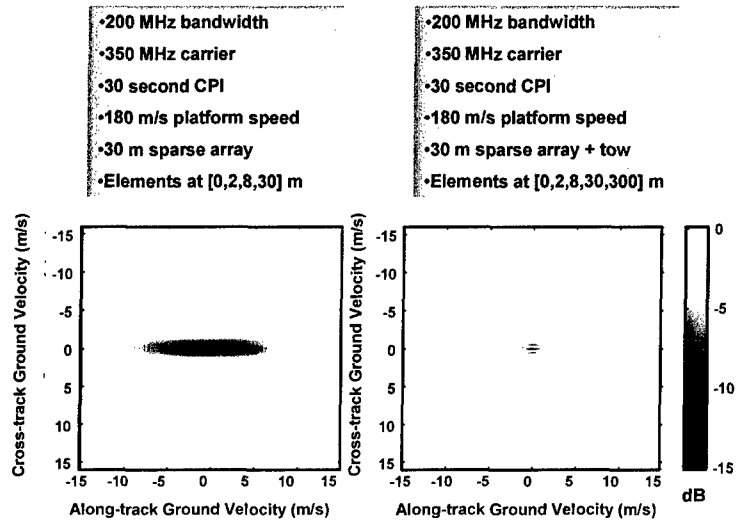


Figure 14. USASTAR SINR loss predictions showing the effect of extending the antenna baseline with a towed aperture 300 m behind the first antenna element, at UHF.

## 4. HIGH-RESOLUTION ADAPTIVE ARRAY PROCESSING APPROACHES

Airborne GMTI radar operation confronts many technological challenges. Most of all, the radar signal processing must cancel strong ground clutter interference with a large Doppler bandwidth in order to detect slowly moving ground targets. Typically, such a task is accomplished by utilizing a receiving array of many phase centers and multichannel receivers that are followed by adaptive array processing. To achieve good clutter cancellation performance in a realistic field operational environment, the processing algorithms must overcome many practical difficulties. For example, different channels of the receiver system may not be well matched. The array response may be distorted as a result of near-field array-airframe interactions. Furthermore, the clutter reflection from the ground is typically not only strong but also heterogeneous due to various terrain types under radar illumination and various discrete and diffuse surface scatterers.

Mathematically, good adaptive array processing performance requires accurate estimation of the clutter covariance matrix  $R$  and the actual array response  $v$  to a target. In practice,  $R$  is substituted by its sample covariance matrix computed or trained with sufficient clutter samples that should be many multiples of the dimensionality of the data vector to avoid excessive estimation loss. These training samples must be statistically identical to the true clutter to be canceled that is imbedded in the test data vector  $z$ , a condition very difficult to satisfy, especially in a heterogeneous, nonstationary ground clutter environment. The estimation of  $R$  also may be plagued by the presence of other interfering targets or target like signals in the clutter training ensemble that cause undesirable mutual target interference. Furthermore, the phase response to a target across the linear receiving array will be distorted due to the strong near-field multipath interactions between the array and the airframe or other anomalies, including mismatched frequency response among different radar channels.

Nonlinear array phase distortion is a serious concern. The adaptive array processor is normally tuned to the desired target signal whose array response must be precisely known. To achieve both high signal gain and clutter cancellation, one must calibrate the array response to accurately predict the array signal attributed to a target.

In this section, several adaptive algorithms will be described to achieve superb clutter cancellation and GMTI detection performance in either radar range-Doppler or SAR image domain. One algorithmic approach utilizes an adaptive matched filter (AMF) that is matched to the array response to the expected target as derived from local clutter eigenvector. This algorithm employs a "local" array calibration process to extract moving target signal in the endo-clutter region but is unable to derive the array target response in the exo-clutter region without clutter data. A similar but different approach implements the single-cell AMF into two steps. Initially, a "global" array calibration matrix used for correcting array distortion is derived from radar range-Doppler clutter data via a least-square procedure. Next, the calibrated target steering vector is incorporated in the AMF to achieve high array SINR improvement in both endo- and exo-clutter regions. A different category of more complicated multicell algorithms capable of better clutter suppression also will be defined. One type is a generalized matched filtering process in the two-dimensional space-fast-time domain that processes additional fast-time range-delay data samples in each array element channel. Another technique of a similar approach is a two-dimensional, multiple-pixel clutter whitening process incorporating a noise-canceling scheme.

A common starting point of all these algorithms is a high-resolution multichannel data set. Given a stream of range-pulse data from each receiving array channel, a range-Doppler map or SAR image is initially formed by integration over a long CPI. Later, several or all of the data maps or images from multiple array channels are to be adaptively combined to achieve the desired clutter cancellation and

target detection results. The adaptive array processing techniques to be explored here may be viewed as different element-space, post-Doppler adaptive array beamforming processes. In actual implementations of Doppler filtering or SAR imaging, coherent integration is performed over a relatively long CPI. The long CPI results in improved radar Doppler or cross-range resolution. Thus, more clutter training samples will be available from the neighborhood of a test target cell to better estimate clutter covariance. In practice, the number of local clutter training samples may approach 100 times the data vector dimension. The large clutter sample size facilitates a very useful data target excising, which is a selective training procedure found to be very effective in mitigating the mutual target interference. High-resolution range-Doppler or SAR image data also provide sufficient clutter samples to support local array calibration that may correct array response distortion in fine elevation and azimuth angle increments. The opportunity for fine-grain local calibration is one important element that results in good adaptive array processing performance.

There is no fundamental distinction between radar range-Doppler and SAR image processing except for the motion compensation applied to radar data. The SAR imaging is a process that maps ground scatterers onto the radar range and cross range data domain by applying precise aircraft motion compensation via a suitable mapping technique such as the backprojection image formation. On the other hand, fast Fourier transform (FFT)-based Doppler filtering is commonly applied in range-Doppler processing to radar range-gated data in order to transform the ground onto a range-Doppler map. Because the integration is carried out over a long CPI, appropriate motion compensation also may be necessary in range-Doppler processing. The compensation could be only approximately and reasonably accurate but not necessarily exact; otherwise, range-Doppler processing essentially becomes synonymous with SAR image processing.

#### **4.1 SINGLE-CELL ADAPTIVE MATCHED FILTERING WITH "LOCAL" ARRAY CALIBRATION**

The adaptive processing algorithms, emphasized in this report, generally belong to a category known as element-space post-Doppler adaptive beamforming. In particular, the Doppler filtering step prior to array beamforming is applied to a full range of radar pulse data. The coherent integration is carried out over a relatively long CPI to increase target signal gain and better prepare high-resolution radar data for further adaptive processing. The long-CPI Doppler filtering necessitates several essential procedures in the signal processing chain to ensure good clutter suppression and GMTI target detection. These procedures include pulse data phase correction for motion compensation, local data-selective training for sample clutter covariance estimation, and array calibration. Due to the radar aircraft motion, the Doppler shift of a scatterer changes appreciably over a long CPI. To correct the Doppler drift, quadratic phase compensation as a primitive form of SAR processing is applied to the pulse train prior to Doppler filtering. The selective training is a procedure that iteratively runs the same adaptive algorithms more than twice. During the initial iteration, a low detection threshold is set to select all potential moving targets in the test data output. The initial detection result is used to selectively delete all potential moving targets from the clutter covariance training data in subsequent runs.

The local array calibration procedure may be integrated as part of the post Doppler adaptive array processing. Given an array data vector  $z$  of dimension  $N$  to be tested for the presence of a target signal  $v$  at the range  $r$  and the Doppler  $f_d$ , one initially estimates the local clutter covariance matrix  $R$  and its principal eigenvector  $u$ , then the AMF output power  $S_{AMF}$  is computed by using



$$\begin{aligned}
S_{AMF} &= \frac{|\mathbf{v}^H \mathbf{R}^{-1} \mathbf{z}|^2}{\mathbf{v}^H \mathbf{R}^{-1} \mathbf{v}} \quad ; \quad \mathbf{R} = \frac{1}{K} \sum_{k=1}^K \mathbf{x} \mathbf{x}^H \quad ; \\
v_n &= u_n \exp \left( j 2 \pi \frac{nd}{\lambda} \cos \theta (\sin \phi_t - \sin \phi_d) \right) \quad , \quad n = 0, 1, 2, \dots, N-1 \quad ; \\
\mathbf{v} &= [1 \ ; \ v_1 \ \dots \ v_n \ \dots \ v_{N-1}] \quad ; \quad \mathbf{u} = [1 \ ; \ u_1 \ \dots \ u_n \ \dots \ u_{N-1}] \quad ; \quad f_d = \frac{2v_a}{\lambda} \cos \theta \sin \phi_d \quad .
\end{aligned} \tag{4.1}$$

In Equation (4.1), the notation denotes the radar wavelength as  $\lambda$ , the array element spacing as  $d$ , the depression angle as  $\theta$ , that varies with the target range  $r$  and the aircraft altitude  $H$  as  $\sin^{-1}(H/r)$ . The azimuth angle  $\phi_d$  of radar line-of-sight (LOS) directed to the range-Doppler cell relative to the array broadside may be calculated from the target Doppler  $f_d$ , the aircraft speed  $v_a$ , and  $\lambda$  as shown. The sample clutter covariance matrix  $\mathbf{R}$  is computed from sufficient sample data vectors  $\mathbf{x}$  selected from the neighborhood of the range-Doppler cell  $\mathbf{z}$  under test. The principal eigenvector  $\mathbf{u}$  of  $\mathbf{R}$  captures the distorted array response specific to the direction as defined by the LOS depression angles  $\theta$  and  $\phi_d$ . The target steering vector  $\mathbf{v}$  is modeled such that its  $n$ th vector component is the product of the corresponding components of an ideal linear array response vector and the principal clutter eigenvector  $\mathbf{u}$ . For each beam position  $\phi$ , one set of AMF output is computed for all range-Doppler cells.

It is intuitively clear that the post-Doppler processing procedures can be readily extended to multichannel SAR processing by replacing the range-Doppler map for each element channel with its equivalent SAR image in the slant-range and cross-range coordinates. The SAR processor accounts for all range and Doppler migration over the entire CPI due to along-track aircraft motion, thereby achieving higher coherent signal gain and better cross-range image resolution from along-track integration. Usually, the radar pulse returns for each channel are independently processed via fast backprojection into a complex, co-registered SAR image by using identical pixel coordinates. Moving target signature may exhibit a certain amount of cross-range coordinate shifting, defocusing, and smearing in the SAR image integrated over the CPI, but otherwise differ from stationary clutter by virtue of the phase progression between channels. In this case, SAR images from multiple channels are processed to calculate the AMF statistic similar to Equation (4.1)

$$S_{AMF} = \max_{v_t} \left( \frac{|\mathbf{v}^H \mathbf{R}^{-1} \mathbf{z}|^2}{\mathbf{v}^H \mathbf{R}^{-1} \mathbf{v}} \right) \quad ; \quad v_n = u_n \exp \left( j 2 \pi \frac{nd}{\lambda} \frac{v_t}{v_a} (\sin \phi_t - \sin \phi_d) \right) \quad . \tag{4.2}$$

Because the target velocity parameter  $v_t$  is unknown, the AMF test statistic is maximized across all possible target velocities. Note that, Equation (4.2) is the same as Equation (4.1) except for a functional change in  $\mathbf{v}$  by invoking the matched target and clutter Doppler condition,  $v_t/v_a = \cos \theta (\sin \phi_t - \sin \phi_d)$ .

Although the single-cell AMF incorporating “local” array calibration results in excellent clutter suppression, this approach is inapplicable to the clutter-free region because no clutter data are available for array calibration. This deficiency motivates an alternative “global” calibration technique that enables the application of new single- and multiple-cell AMF algorithms to both the endo- and the exo-clutter regions. These AMF processes will be analyzed in detail following the discussion of the array calibration procedure.

## 4.2 ARRAY RESPONSE CALIBRATION

The guiding principle of correcting the array distortion is to derive an  $N \times N$  constant matrix  $C$  that linearly relates the actual array data  $a(\phi)$  in the direction  $\phi$  to the ideal array response  $v_i(\phi)$  as  $a(\phi) = C v_i(\phi)$  or conversely,  $v_i(\phi) = C^{-1} a(\phi)$ . Because numerous clutter cells are available in a high-resolution range-Doppler map, one may accurately estimate  $C$  via the standard least-square procedure by adopting a measurement data model  $X = CV + E$ . The data matrix  $X = [a(\phi_1), \dots, a(\phi_k), \dots]$  consists of  $K$  range-Doppler clutter data vector  $a(\phi_k)$ ,  $k = 1, 2, \dots, K$ ,  $V = [v_i(\phi_1), \dots, v_i(\phi_k), \dots]$  is a similar matrix of  $K$  ideal Vandermonde vectors,  $v_i(\phi_k)$ ,  $k = 1, 2, \dots, K$ , and the Gaussian matrix  $E$  models the measurement errors. Assuming an aircraft speed  $v_a$  and a depression angle  $\theta$  that is range-dependent, the azimuthal angle  $\phi_k$  of a range-Doppler clutter cell is related to its Doppler  $f_d$  by  $f_d = (2v_a/\lambda)\cos\theta\sin\phi$ . In this formulation, the  $C$  matrix is estimated from  $X$  as follows:

Array calibration model:

$$\alpha(\theta) = C v_i(\theta) \quad \text{or} \quad v_i(\theta) = C^{-1} \alpha(\theta) ; \quad C \text{ is } \theta \text{ dependent.}$$

$$v_i(\theta) = [1 ; \alpha ; \alpha^2 \dots \alpha^{N-1}] ; \quad \alpha = \exp\left(j2\pi \frac{d}{\lambda} \cos\theta \sin\phi\right) .$$

Measurement data model:

(4.3)

$$X = CV + E ;$$

$$X = [a(\phi_1) \quad a(\phi_2) \quad \dots \quad a(\phi_k) \quad \dots \quad a(\phi_K)] , \quad k = 1, 2, \dots, K ;$$

$$V = [v_i(\phi_1) \quad v_i(\phi_2) \quad \dots \quad v_i(\phi_k) \quad \dots \quad v_i(\phi_K)] , \quad k = 1, 2, \dots, K ;$$

$$\text{LMS estimate of } C: \quad C = XV^H (VV^H)^{-1} .$$

In practice, a separate calibration matrix  $C$  is estimated for each range gate to account for the elevation angle dependence of the array response. This technique has proved to be very effective and satisfactory in correcting the array response distortion. The data vector  $a(\phi)$  in Equation (4.3) also may be replaced by the principal eigenvector of the local clutter covariance  $R$ , but negligible improvement is expected should the clutter-to-noise measurement be high enough.

## 4.3 SINGLE-CELL ADAPTIVE MATCHED FILTERING WITH “GLOBAL” ARRAY CALIBRATION

Once completing the array calibration procedure, the single-cell post-Doppler AMF detection amplitude  $z_{AMF}$  is now calculated from Equation (4.1) by using the calibrated array signal  $v = C v_i$  as derived from the ideal target steering vector  $v_i$

$$\begin{aligned}
z_{AMF} &= \frac{\mathbf{v}^H \mathbf{R}^{-1} \mathbf{z}}{\sqrt{\mathbf{v}^H \mathbf{R}^{-1} \mathbf{v}}} \quad ; \quad z_{MVDR} = \frac{\mathbf{v}^H \mathbf{R}^{-1} \mathbf{z}}{\mathbf{v}^H \mathbf{R}^{-1} \mathbf{v}} \quad ; \\
\mathbf{R} &= \frac{1}{K} \sum_{k=1}^K \mathbf{x} \mathbf{x}^H \quad ; \quad \mathbf{v}(\theta) = \mathbf{C} \mathbf{v}_t(\theta) \quad ; \\
\mathbf{v}_t(\theta) &= [1 \quad ; \quad \alpha \quad ; \quad \alpha^2 \quad \dots \quad \alpha^{N-1}] \quad ; \quad \alpha = \exp \left( j 2 \pi \frac{d}{\lambda} \cos \theta \sin \phi_t \right) .
\end{aligned} \tag{4.4}$$

In Equation (4.4), the AMF filter output is specified by a complex amplitude  $z_{AMF}$  instead of the power  $S_{AMF}$  in Equation (4.1). In addition, the corresponding minimum variance distortionless response (MVDR) filter amplitude  $z_{MVDR}$  is specified that is normalized differently as an unbiased estimate of the signal amplitude.

#### 4.4 MULTIPLE-CELL SPACE-FAST-TIME ADAPTIVE MATCHED FILTERING

While the previous single-cell post-Doppler AMF or MVDR filter is capable of substantial clutter suppression, further improvement may be realized by passing the MVDR output through a Wiener noise cancellation filter. The Wiener filter (WF), structured as a sidelobe canceller, correlates, estimates, and partially cancels the residual interference imbedded in the MVDR output  $z_{MVDR}$  with an auxiliary data set  $y$  that assembles range-delayed copies of the original multichannel range-Doppler data vector  $x$ . Explicitly, for each array data vector  $x$  at a range-Doppler cell, a corresponding  $y$  data vector is created by concatenating several  $x$ -vectors of adjacent range gates. For example, given  $M$  range-delayed taps centered at the range-Doppler cell  $rd$ ,  $M \times$  vectors of dimension  $N$  may be stacked as  $y_{rd} = \text{vec}([x_{r-M/2,d} \dots x_{r-1,d} \quad x_{r+1,d} \dots x_{r+M/2,d}])$ ; typically,  $M$  may be fixed at 4 to 6 in practical data processing. Using the auxiliary data  $y$  of dimension  $MN$ , the detection statistic  $z_{WF}$  out of the cascaded MVDR and Wiener filters is derived from the data vector  $z$  of the test target cell as

$$\begin{aligned}
z_{MVDR} &= \frac{\mathbf{v}^H \mathbf{R}^{-1} \mathbf{z}}{\mathbf{v}^H \mathbf{R}^{-1} \mathbf{v}} \quad ; \quad z_{WF} = z_{MVDR} - \mathbf{R}_{zy} \mathbf{R}_{yy}^{-1} y \quad ; \\
\mathbf{R} &= \frac{1}{K} \sum_{k=1}^K \mathbf{x} \mathbf{x}^H \quad ; \quad \mathbf{R}_{zy} = \frac{1}{K} \sum_{k=1}^K z_{MVDR} y^H \quad ; \quad \mathbf{R}_{yy} = \frac{1}{K} \sum_{k=1}^K y y^H .
\end{aligned} \tag{4.5}$$

Auxiliary data vector  $y_{rd}$  at the range-Doppler cell  $rd$ :

$$y_{rd} = \text{vec} \left( \begin{bmatrix} \mathbf{x}_{r-M/2,d} & \dots & \mathbf{x}_{r-1,d} \mathbf{x}_{r+1,d} & \dots & \mathbf{x}_{r+M/2,d} \end{bmatrix} \right) .$$

The procedure used for estimating the covariance matrices,  $\mathbf{R}_{zy}$  and  $\mathbf{R}_{yy}$ , is identical to the previous scheme used for estimating the covariance  $\mathbf{R}$  of  $x$ . Note that the adaptive processing DoF is now equal to the dimension of the  $y$  vector as the product of the array size  $N$  and the number of range-delay taps  $M$ .

The cascaded MVDR and Wiener filter structure, defined by Equation (4.5), actually is actually a suboptimal rendition of one optimal process. The optimal process, referred here as multiple-cell adaptive matched filter, swaps the order of execution of the MVDR and the Wiener noise cancellation filters. This novel algorithm is applicable to any situation whenever a set of auxiliary interference plus noise data  $y$  are available such that  $y$  is free of the target signal and is correlated with the primary interference process  $x$ . In the current application,  $y$  is created by stacking multiple copies of the range-delayed array data vector  $x$  adjacent to the test target range cell in the range-Doppler domain as previously explained. Thus, adaptive

processing is applied to the two-dimensional data vectors sampled in space by different array elements and in fast time by different range gates.

Assuming that the auxiliary data  $y$  may suitably be modeled as a complex Gaussian vector process, one may derive the structure of the optimal multiple-cell adaptive matched filter and its detection statistic by performing the standard hypothesis test on the composite data vector  $z_c = [z ; y]$  to determine the presence or absence of a target in the test data vector  $z$  or equivalently  $z_c$ . Under the target hypothesis  $H_1$ ,  $z = sv + x$  is the superposition of both a target signal  $sv$  and the interference vector  $x$ , and it follows that  $z_c = [sv + x ; y]$ . Whereas under the null hypothesis  $H_0$ ,  $z = x$  consists of only the interference  $x$  and  $z_c = [x ; y]$ . Based on these modeling assumptions, the generalized likelihood ratio test computes the output detection statistic  $z_{MVDR}$  or  $z_{AMF}$  of the multiple-cell MVDR or AMF algorithm as follows.

Two-step filtering process:

$$\text{Wiener noise cancellation: } z_u = z - R_{xy}R_{yy}^{-1}y ;$$

$$\text{MVDR filtering: } z_{MVDR} = \frac{v^H R_{uu}^{-1} z_u}{v^H R_{uu}^{-1} v} ; \left( \text{or AMF } z_{AMF} = \frac{v^H R_{uu}^{-1} z_u}{\sqrt{v^H R_{uu}^{-1} v}} \right) ; \quad (4.6)$$

$R_{uu}$  is the covariance of residual interference  $u$  after Wiener filtering:

$$u = x - R_{xy}R_{yy}^{-1}y ; \quad R_{uu} = R_{xx} - R_{xy}R_{yy}^{-1}R_{yx} ;$$

$$R_{xx} = \frac{1}{K} \sum_{k=1}^K xx^H ; \quad R_{xy} = \frac{1}{K} \sum_{k=1}^K xy^H ; \quad R_{yy} = \frac{1}{K} \sum_{k=1}^K yy^H .$$

The multiple-cell AMF or MVDR processing as defined by Equation (4.6) uses an extended array target steering vector  $[v ; 0]$  of higher dimension, whose subspace projection  $v$  is identical to that used in the single-cell AMF or MVDR filter. Although the processing steps of the current algorithm are well defined, the assumption of the absence of any target signal in the auxiliary training data  $y$  is critical and must be satisfied to achieve high interference cancellation. The computational load of the multiple-cell algorithm is expected to be higher than its single-cell counterpart due to increasing adaptive processing DoFs, now equal to the dimension of the composite data vector  $[x ; y]$  instead of the  $x$  data vector.

#### 4.5 MULTIPLE-PIXEL ADAPTIVE SAR IMAGE PROCESSING

A similar multiple-cell noise whitening process also may achieve high clutter suppression performance. This scheme is motivated by the realization that the signature of a moving target may be smeared after integration over a long CPI. The signal smearing, often neglected in the preceding single-cell AMF processing, spreads target information across multiple radar range-Doppler cells or SAR range and cross-range pixels in each channel. For this reason, adaptive algorithm performance can be improved by processing the extended image data vectors  $z_e$  constructed by concatenating multiple data vectors  $z$  of adjacent cells. The current SAR image whitening filter, carried out in the extended, multiple-pixel vector space, does not employ a target model but incorporate a “noise subtraction” process:

$$S_{\text{whitening}} = z_e^H R^{-1} z_e - z_e^H R_N^{-1} z_e ;$$

$$(R_N)_{ij} = \begin{cases} (R)_{ij} & \text{for } i \text{ and } j \text{ form the same receiving array element} ; \\ 0 & \text{for } i \text{ and } j \text{ form different receiving array elements} . \end{cases} \quad (4.7)$$

Conceptually, the output of the multiple-pixel (or multiple-cell) whitener consists of contributions from (a) same-pixel, cross-element terms, (b) cross-pixel, cross-element terms, and (c) cross-pixel, same-element terms. The first term represents information produced by single-pixel whitening. The second term supplies useful new information about moving targets not available with single-pixel whitening. The third pixel-space whitening term does not carry information about moving targets but tends to accentuate the noise level after the sample covariance matrix inversion. One possible remedy is to perform noise subtraction by employing a noise covariance  $R_N$  that is constructed from  $R$  by zeroing all its cross-element entries. Consequently, the subtraction in Equation (4.7) should cancel the purely pixel-space whitening common to both  $R$  and  $R_N$  while leaving the cross-element whitening terms intact. Mathematically, one may regard Equation (4.7) as the outcome of a maximum likelihood ratio test designed to test the presence of a random Gaussian target signal vector that is characterized by a covariance matrix  $R$ , against the target-absent data that are instead characterized by a noise covariance  $R_N$ .

#### 4.6 SAMPLE RADAR MEASUREMENT RESULT

One sample result of the multiple-cell AMF incorporating four range-delayed taps is depicted in Figure 4.1 to highlight its excellent performance in clutter cancellation. The data used in this example were gathered by the Tuxedo radar of the Lockheed Martin Corporation, M&DS Reconnaissance System in 1999 under the DARPA Discoverer II Program [4]. The Tuxedo radar antenna has three horizontally polarized subarray apertures; each subarray spans 0.61 m in length. One subarray is stacked on top of the other two adjacent subarrays so that the total azimuthal aperture length is 1.22 m. Such a structure yields the azimuthal beamwidth of 3.6 deg and the elevation beamwidth of 9.1 deg. The antenna gain is 26.7 dBi. The particular data set under discussion was gathered in Pass 1916 by the Tuxedo radar in its spotlight mode. The radar was operated at the center frequency of 9600 MHz with a 300 MHz bandwidth and the radar pulse PRF was 1363 Hz. However, the data bandwidth was reduced to 180 MHz for this adaptive processing exercise. In addition, the data pre-processing procedures also included channel equalization over the operational bandwidth and rudimentary motion compensation to correct antenna phase relative to a fixed aim point on the ground. During the data collection, the radar flew at the approximate altitude of 5982 m at the speed of 136 m/s. Five ground moving vehicles were deployed for measurement, including a HMMWV, a 2.5-ton truck, a 5-ton truck, a large fuel truck, and a PLS.

Figure 15(a) shows the range-Doppler map of one channel after coherent integration of 0.75 s. Prior to Doppler filtering, clutter amplitude has been limited at the maximum of 30 dB above noise without alternation of its phase. The range-Doppler map of the clutter scene generally reflects the test ground that has many flat surface, roads, and fixed structures such as buildings. The map indicates the average element clutter-to-noise ratio within the mainbeam region is below 20 dB. However, the discrete clutter strength is much stronger and may exceed 40 dB. Figure 15(b) plots the output of the multiple-cell MVDR process from Equation (4.6) that depicts the signal-to-residual-clutter-plus-noise ratio in the same dynamic range and over the same target area as that in the Figure 15(a). The ability of this adaptive process to cancel ground clutter and to improve the test target signatures is apparent. The binary detection map of the Figure 15(c) is obtained by applying a sufficiently high detection threshold to the output MVDR statistics such that no false alarm appears in the data domain. In this example, four out of five moving vehicles are detected. A range-cut of the data result cross the slowest target at the range of approximately 21.7 km is illustrated in the Figure 15(d). Note that the slowest target being detected moves at the approximate speed of 0.5 m/s.

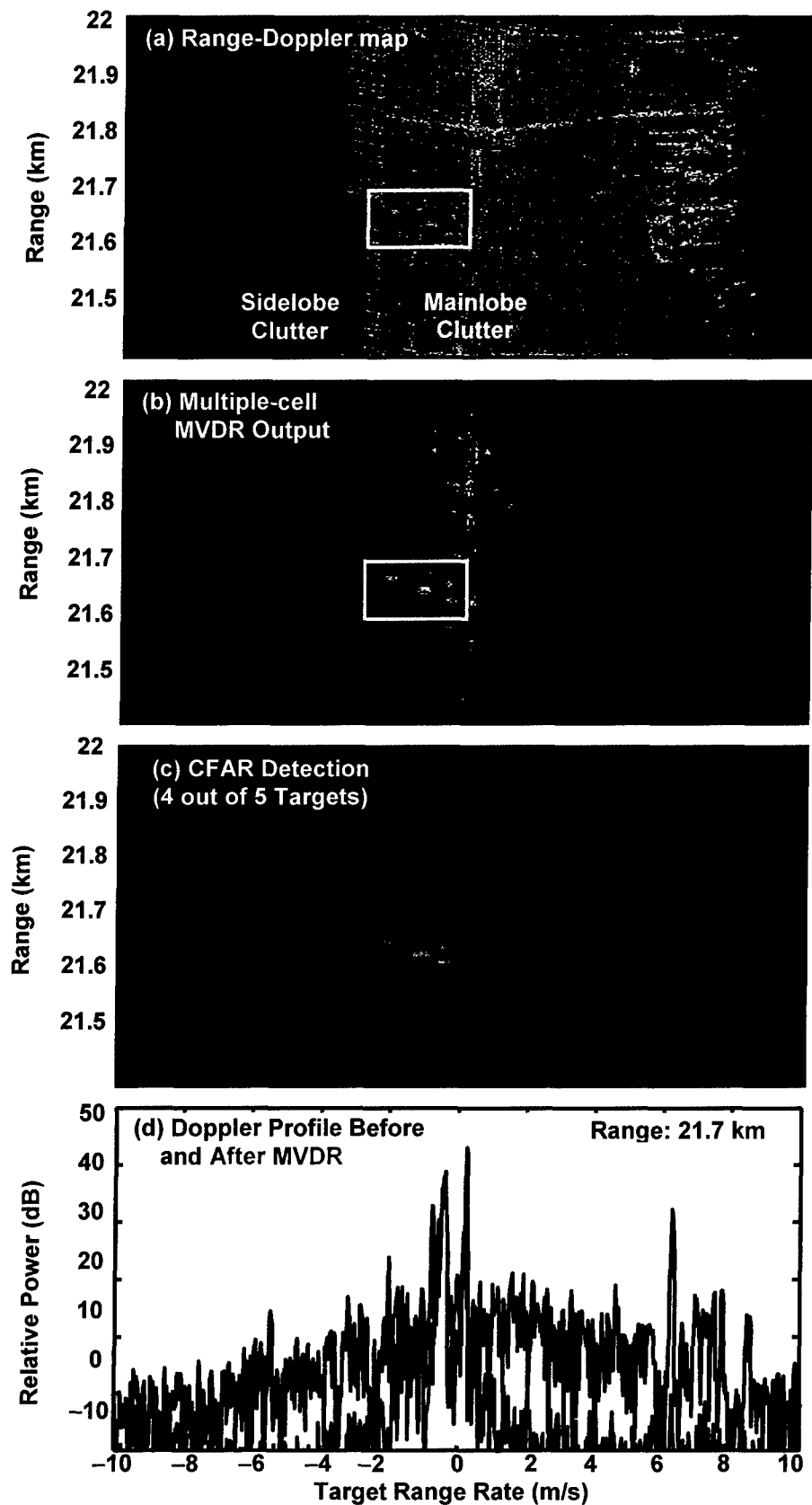


Figure 15. Sample output of the multiple-cell adaptive processing derived from the Tuxedo data set No. 1916 over a test area.

## 5. SUMMARY

A unified SAR and GMTI radar concept, USASTAR has been described in this report. USASTAR provides a standoff, rapid wide area search radar concept with capability to detect small targets that are stationary or moving at arbitrary speed and direction simultaneously. The novel concept is based on large baseline multichannel SAR adaptive clutter cancellation, while minimizing target signal losses. Target signal losses are minimized by operating with wideband waveforms and antenna baselines that are so long that targets move two or more resolution cells during the time the platform flies the length of the antenna baseline. The required antenna baseline can be too long to be satisfied with filled apertures, but the USASTAR technique would work with very sparse arrays such as two separate antenna arrays carried by two separate platforms flying in tandem, as long as phase coherency between all the antenna phase centers is assured by accurate antenna position measurements.

Theoretical frameworks formulating the USASTAR concept and its performance are provided in this report. Performance predictions are presented in terms of predicted target signal loss, or SINR loss, with UHF and X-band USASTAR parameters. Also presented are algorithms for USASTAR clutter cancellation and target detection. These algorithms were successfully tested against Tuxedo multichannel X-band data on moving ground targets. Vehicle targets in the open were detected at a radial speed as slow as 0.5 m/sec. Example Tuxedo X-band results are presented.

## REFERENCES

1. J.K. Jao, "Theory of Synthetic Aperture Radar Imaging of a Moving Target," *IEEE Trans. on Geoscience and Remote Sensing*, Vol. 39, No. 9, 1984–1992 (September 2001).
2. J.K. Jao, "SAR Image Processing for Moving Target Focusing," *Proc. of the 2001 IEEE Radar Conf.*, Atlanta, GA, 58–63 (1–3 May 2001).
3. A.F. Yegulalp, "Analysis of SAR Image Formation Equations for Stationary and Moving Targets," MIT Lincoln Laboratory, Lexington, MA, Project Report FPR-14 (20 June 2002).
4. P.J. Wagner and L.D. Thompson, "Tuxedo Airborne Testbed," Lockheed Martin M&DS-Reconnaissance Systems Presentation (2 June 1999).
5. A.F. Yegulalp, "Wide Band–Long CPI GMTI," *12<sup>th</sup> Adaptive Sensor Array Processing Workshop*, MIT Lincoln Laboratory, Lexington, MA (16–18 March 2004).



REPORT DOCUMENTATION PAGE				Form Approved OMB No. 0704-0188		
<p>The public reporting burden for this collection of information is estimated to average 1 hour per response, including the time for reviewing instructions, searching existing data sources, gathering and maintaining the data needed, and completing and reviewing the collection of information. Send comments regarding this burden estimate or any other aspect of this collection of information, including suggestions for reducing the burden, to Department of Defense, Washington Headquarters Services, Directorate for Information Operations and Reports (0704-0188), 1215 Jefferson Davis Highway, Suite 1204, Arlington, VA 22202-4302. Respondents should be aware that notwithstanding any other provision of law, no person shall be subject to any penalty for failing to comply with a collection of information if it does not display a currently valid OMB control number.</p> <p><b>PLEASE DO NOT RETURN YOUR FORM TO THE ABOVE ADDRESS.</b></p>						
1. REPORT DATE (DD-MM-YYYY) 24 May 2004		2. REPORT TYPE Project Report		3. DATES COVERED (From - To)		
4. TITLE AND SUBTITLE  Unified Synthetic Aperture Space Time Adaptive Radar (USASTAR) Concept				5a. CONTRACT NUMBER F19628-00-C-0002		
				5b. GRANT NUMBER		
				5c. PROGRAM ELEMENT NUMBER		
				5d. PROJECT NUMBER 1		
6. AUTHOR(S)  J. K. Jao, A. F. Yegulalp, and S. Ayasli				5e. TASK NUMBER 9615		
				5f. WORK UNIT NUMBER		
7. PERFORMING ORGANIZATION NAME(S) AND ADDRESS(ES) Lincoln Laboratory, MIT 244 Wood Street Lexington, MA 02420-9108				8. PERFORMING ORGANIZATION REPORT NUMBER NTI-4		
9. SPONSORING/MONITORING AGENCY NAME(S) AND ADDRESS(ES) Air Force Electronic Systems Command/XPK 5 Eglin Street Hanscom AFB, MA 01731				10. SPONSOR/MONITOR'S ACRONYM(S)		
				11. SPONSOR/MONITOR'S REPORT NUMBER(S) ESC-TR-2003-085		
12. DISTRIBUTION/AVAILABILITY STATEMENT Approved for public release; distribution is unlimited.						
13. SUPPLEMENTARY NOTES None						
14. ABSTRACT A novel airborne GMTI radar approach based on adaptive multichannel SAR processing is proposed to improve the surface surveillance sensor performance in detecting slowly moving targets on the ground. The key sensor attributes are broad bandwidth, large antenna array baseline of multiple phase centers, and adaptive array processing over a long coherent integration time interval. This sensor architecture may improve the GMTI sensor capabilities in several aspects 1) Target detection at very low minimum detectable velocity (MDV) 2) Robust adaptive processing to cancel strong ground clutter 3) High sensitivity to detect weak targets 4) Flexible array requirement including sparser arrays 5) Compatibility with SAR imaging applications. The presented sensor architecture is suitable for deployment on a fast, stand-off airborne surveillance platform against weak and slow targets such as dismounted troops, guerrillas, terrorists, and illegal vehicle or boat traffic, both in the clear and under concealment.						
15. SUBJECT TERMS						
16. SECURITY CLASSIFICATION OF:			17. LIMITATION OF ABSTRACT	18. NUMBER OF PAGES	19a. NAME OF RESPONSIBLE PERSON	
a. REPORT	b. ABSTRACT	c. THIS PAGE	None	37	19b. TELEPHONE NUMBER (Include area code)	
Unclassified	Unclassified	Unclassified				